Effects of Voltage sag on Doubly Fed Induction Machine at Hyper-Synchronous Motoring Mode

Navneet Kumar, Thanga Raj Chelliah
Department of WRD&M
Indian Institute of Technology
Roorkee, India
teenvan2002@gmail.com, thangaraj@ieee.org

S.P. Srivastava
Department of Electrical Engineering
Indian Institute of Technology
Roorkee, India
satyafee@iitr.ernet.in

***Abstract*—Load-frequency match is mandatory requirement for interconnected power system stability. Any unscheduled change in load or intermittent power injection from Renewable Energy Sources (RES) leads to system instability by changing the frequency. Therefore, energy storage devices are essential as they can provide quick response for any change in system frequency. Pumped Storage Plants (PSP) serves the dual purpose, either by storing surplus power or by generating hydro power during peak requirements. The use of Doubly-Fed Induction Machine (DFIM) with power electronics in rotor circuit is significant in both motoring and generating modes in PSP. This paper investigates the effect of symmetrical voltage sag on the performance of DFIM at motoring mode. Various motor parameters, namely peaks in total power taken from grid, torque and current (stator and rotor current), and speed loss were investigated. With the aid of both simulation and experimental results, symmetrical voltage sag effects on a 2.2kW three-phase DFIM are analyzed. In steady-state operation of DFIM, the voltage sag produces motor instability which depends on sag depth and duration.**

Keywords— Doubly-fed induction machine, Pump storage scheme, Reactive power control, Speed control, Symmetrical voltage sag;

I. INTRODUCTION

With the strict rule-regulation guideline form government agencies for environmental awareness worldwide, more attention has been paid to cheap and clean energy generation in past few years. Various attempts have been made by researchers for expansion in the use of various types of RES. Continuous growth can achieve emission cut objective from conventional power generation, by reducing the greenhouse gas emission to zero [1-3]. Since uncertainty and volatility is always allied with RES, so high power fluctuation in interconnected grid system is noticed. To overcome such power fluctuation, energy storage devices are essential to play an important role for power storage and generation as well during peak demands. Bulk power storage available with PSP, batteries, superconducting magnet energy storage, flywheel energy storage, regenerative fuel cell storage and compressed air energy storage have been reported in literature [4]. Commercially, cheap and large capacity (both quantity and duration) of energy storage is available with PSP [5]. Quick response of PSP for unscheduled change in system loading is achieved by variable speed pump-turbine operation. Although overall operation (motoring and generating) of PSP consumes energy, but it provides more power system stability and revenues are generated by selling high price electricity during peak demand periods.

Variable speed pump-turbine operation in PSP is obtained either by synchronous machine (either electrical or permanent magnet excitation) or by DFIM [6, 7]. These machines offers several advantages including active power control in pumping mode, reactive power control at the interconnection point and instantaneous active power injection in the grid (flywheel effect) [8, 9]. Now a day, DFIM with power electronics in rotor circuit is an emerging system to generate hydro-power or wind-power efficiently. DFIM offers advantage of Variable Speed Drive (VSD) with four quadrants operation with active, reactive power control and lower power losses and especially the converter cost [10]. DFIM application in PSP is significant in both motoring and generating modes.

A recent survey concluded, about 92% of all process interruptions in power system is caused by voltage sags. The highly sensitive load often trips or shuts down during voltage sag. Therefore, this is essential to understand the behavior of sensitive equipment during voltage sag so that the proper methods for mitigation can be developed.

A. Problem Description

Voltage sag is one of the most severe power quality disturbances to be dealt with by the industrial sector, as it can cause severe process disruptions and results are poor quality products and substantial economic loss. In PSP, variable speed DFIM pump-turbine system is used for water pumping from lower reservoir to high reservoir. During pumping operation, due to voltage sag the process may disturb or stall. This interruption depends upon type, depth and duration of voltage sag.

B. Contribution

Steady state operation of DFIM at hyper-synchronous motoring mode is obtained. Rotor side controller is developed for speed control and stator side reactive power control. During steady state condition, the symmetrical voltage sag (Type-A) is created with different sag depth and sag duration.

Comprehensive analysis is carried out for DFIM operating with voltage sag. Peaks in total power taken from grid, torque and current (stator and rotor current), and speed loss was investigated depending upon various voltage sag depth and duration. A 2.2kW DFIM stable region for operation with 0.75pu torque and 1.1pu speed is also described corresponding to various sag depth and duration.

C. Paper organization

The organization of this paper is as follows. Section II briefly explain the types of voltage sags and variable of interest for study, section III explain DFIM modelling and speed control along with stator side reactive power control, section IV comprises an effects of voltage sag on DFIM, section V presents the experimental results for effects of voltage sag and the paper concludes at section VI.

II. VOLTAGE SAG CHARACTERIZATION

A. Sag classification

Table I classifies categories of voltage sags according to IEEE standard [11]. Voltage sag (dip) is basically the decrease in rms voltage between 0.1pu and 0.9pu, with duration between 0.5 cycles and 1 min. Voltage sags can be either symmetrical or unsymmetrical, if the individual phase voltages are equal and the phase relationship is 120°, the sag is symmetrical otherwise, the sag is unsymmetrical [12]. This paper deals with only symmetrical voltage sag caused by three phase faults.

It is considered that fault occurred in three phase is cleared instantaneously, and then sag is representation as abrupt (type-A). Voltage sag can be cleared in two or three steps shown in Fig. 1, and then sag is represented as discrete. For symmetrical sage (type-A), these possibilities are denoted by five cases i.e. A_1, A_2, A_3, A_4 and A_5, which can be found in [13]. Fig. 1 shows voltage waveform (RMS) for type-A (abrupt) sag and type A_1 and A_3 (discrete) sag. In general symmetrical sag is described by three parameters, namely sag depth (h), sag duration (Δt) and fault angle current (ψ).

B. Variable of interrest

In this paper, the variables chosen to study behavior of DFIM during voltage sags are the total power, stator currents, rotor currents, torque peaks, and speed loss. All values are calculated in pu quantities.

$$I_{peak(s)}(pu) = \frac{I_{peak(s)}}{\sqrt{2}I_{rated(s)}} = \frac{\max\{|I_{a(s)}(t)|, |I_{b(s)}(t)|, |I_{c(s)}(t)|\}}{\sqrt{2}I_{rated(s)}}$$

$$I_{peak(r)}(pu) = \frac{I_{peak(r)}}{\sqrt{2}I_{rated(s)}} = \frac{\max\{|I_{a(r)}(t)|, |I_{b(r)}(t)|, |I_{c(r)}(t)|\}}{\sqrt{2}I_{rated(s)}}$$

$$\omega_{min}(pu) = \frac{\min\{|\omega(t)|\}}{\omega_{rated}}$$

$$T_{peak}(pu) = \frac{\max\{|T(t)|\}}{T_{rated}}$$

$$P_{peak}(pu) = \frac{\max\{|P(t)|\}}{P_{rated}}$$

TABLE I. TYPE OF VOLTAGE SAG [14]

Categories	Typical Duration (50 Hz)	Typical Voltage Magnitude
Instantaneous sag	0.5 – 30 cycles (10 - 600 msec)	0.1 – 0.9 pu
Momentary sag	30 – 150 cycles (600 msec – 3 sec)	0.1 – 0.9 pu
Temporary sag	150 – 3000 cycles (3 sec – 60 sec)	0.1 – 0.9 pu

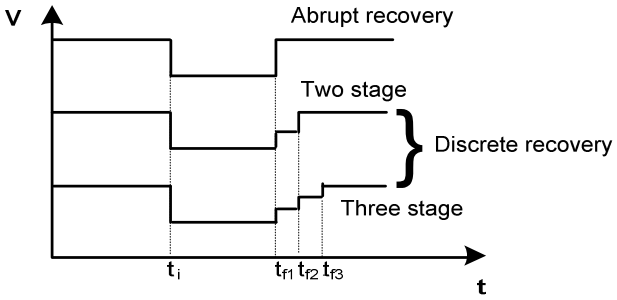

Fig. 1 RMS Voltage for abrupt and discreet recovery

III. DFIM MODELLING AND CONTROL

Stator-field-oriented vector control scheme is opted for speed regulation of DFIM in setting speed region, where d-axis is aligned with stator flux and reference frame rotates synchronously with stator flux. The suitable rotor side voltages u_{rd} and u_{rq} are applied thereby to control the rotor d-q axes currents i_{rd} and i_{rq}. Rotor current q-component enabling the machine torque and stator active power is manipulated directly whereas d-component controls the stator reactive power because flux in the machine determined by stator voltage. The rotor side converter control scheme involves two PI control loops: two inner current control loops and two outer control loops for speed and stator reactive power control.

Rotor voltage governing equations can be expressed as [15, 16]:

$$u_{rd} = R_r i_{rd} + \sigma L_r \frac{di_{rd}}{dt} - \omega_{sl}\sigma L_r i_{rq} \quad (1)$$

$$u_{rq} = R_r i_{rq} + \sigma L_r \frac{di_{rq}}{dt} + \omega_{sl}\frac{L_m^2}{L_s} i_{ms} + \omega_{sl}\sigma i_{rd} \quad (2)$$

For Stator-field-oriented vector control, substituting $\psi_{sd} = L_m i_{ms}$ and $\psi_{sq} = 0$, the stator fluxes can be given by:

$$\psi_{sd} = L_s i_{sd} + L_m i_{rd} = L_m i_{ms} = \psi_s,$$

$$i_{ms} = \left[\frac{L_s}{L_m}\right] i_{sd} + i_{rd} \quad (3)$$

$$\psi_{sq} = L_s i_{sq} + L_m i_{rq} = 0 \quad ,$$

$$0 = \left[\frac{L_s}{L_m}\right] i_{sq} + i_{rq} \quad (4)$$

The rotor reference currents i_{rd}^* and i_{rq}^* derived from the outer PI control loops where the errors of the actual and reference stator reactive power and speed are processed [17].

$$i_{rd}^{*} = k_{p(Q)}(Q_s^{*} - Q_s) - k_{i(Q)} \int (Q_s^{*} - Q_s) \frac{L_s}{u_{sq} L_m} + i_{ms} \quad (5)$$

$$i_{rd}^{*} = k_{p(\omega)}(\omega_r^{*} - \omega_r) + k_{i(\omega)}(\omega_r^{*} - \omega_r) \quad (6)$$

Further the cross coupling terms are subtracted for enhancing the response of controller. The generated signals u_{rd}^{*} and u_{rq}^{*} are thereby transformed to rotor phase variables, and desired speed regulation stator reactive power is achieved. The d-q axis rotor voltage is as follows:

$$u_{rd}^{*} = k_{pr}(i_{rd}^{*} - i_{rd}) + k_{ir}(i_{rd}^{*} - i_{rd}) - \omega_{sl} \sigma L_r i_{rq} \quad (7)$$

$$u_{rq}^{*} = k_{pr}\left(i_{rq}^{*} - i_{rq}\right) + k_{ir}(i_{rq}^{*} - i_{rq}) + \omega_{sl} \frac{L_m^2}{L_s} i_{ms} + \omega_{sl} \sigma i_{rd} \quad (8)$$

The principal of vector control can be applied to Grid Side Converter (GSC) also. GSC is used to maintain DC link voltage constant [18] by controlling grid side d-q current components. This fixed DC link voltage works as source for RSC. Governing equation and design of GSC can be found in [19]. Therefore, GSC and RSC are connected through DC link and power can flow in both directions. The direction of rotor power flow depends on mode of operation and settling speed region. Here in this paper simple control scheme is opted for standard one-quadrant motor drive operation. System cost and complexity is reduced by using grid side diode-bridge converter. Hence, for hyper-synchronous speed region, power flow is positive (into rotor circuit) at motoring mode of operation.

IV. Voltage Sag Effects on DFIM

In this study, a 2.2-kW three-phase slip ring induction motor is used as DFIM for simulation and experimental tests, specification is available in Appendix A. DFIM as motor is started by means of three-phase auto-transformer connected to stator windings and two switches S_1 and S_2 shown in Fig. 2. DFIM speed (hyper-synchronous region) is regulated by the vector control scheme by Rotor side converter. DFIM is operating in steady state condition at hyper-synchronous motoring mode for 0.75pu load torque and 1.1pu speed. Symmetrical type-A (abrupt) voltage sag h=0.5, Δt=4T (3.00 – 3.08 sec), ψ=0° is created and the simulation results shown in Fig. 3 shows on-sag and post-sag peaks in (a) stator currents (b) rotor currents (c) torque (d) speed (e) total power taken from grid. Table III shows the effects of voltage sag and duration on the DFIM system.

In experimental test, the voltage sag is achieved by rotating three-phase autotransformer manually. Particular sag depth and duration is achieved by hit and trial method. At time t=50sec, switch S_1 is open and S_2 is closed and speed is regulated. At time t=100sec 50% load is applied to machine and it has been increased to 75% at time t=150sec. Fig. 2 shows the laboratory experimental setup diagram used for analysis of DFIM. Lamp-load connected, 3-hp DC generator is used for load purposes. One quadrant operation of DFIM (hyper-synchronous speed motoring mode) is achieved by Intelligent Power Module (IPM – PEC16DSM01, output RMS current 10Amps) with grid side diode-bridge converter and rotor side PWM controlled converter. Feedbacks are taken from dSPACE-1104 control kit, and high performance control is realized. Hall Effect base sensors are used for measuring voltages and currents and Quadrature Encoder Pulse (QEP) type position encoder (1024 pulse per revolution) is used for speed and position measurement. In steady state for particular voltage sag, drop in RMS grid voltage and stator currents magnitude are measured by FLUKE-435 Power Quality Analyzer.

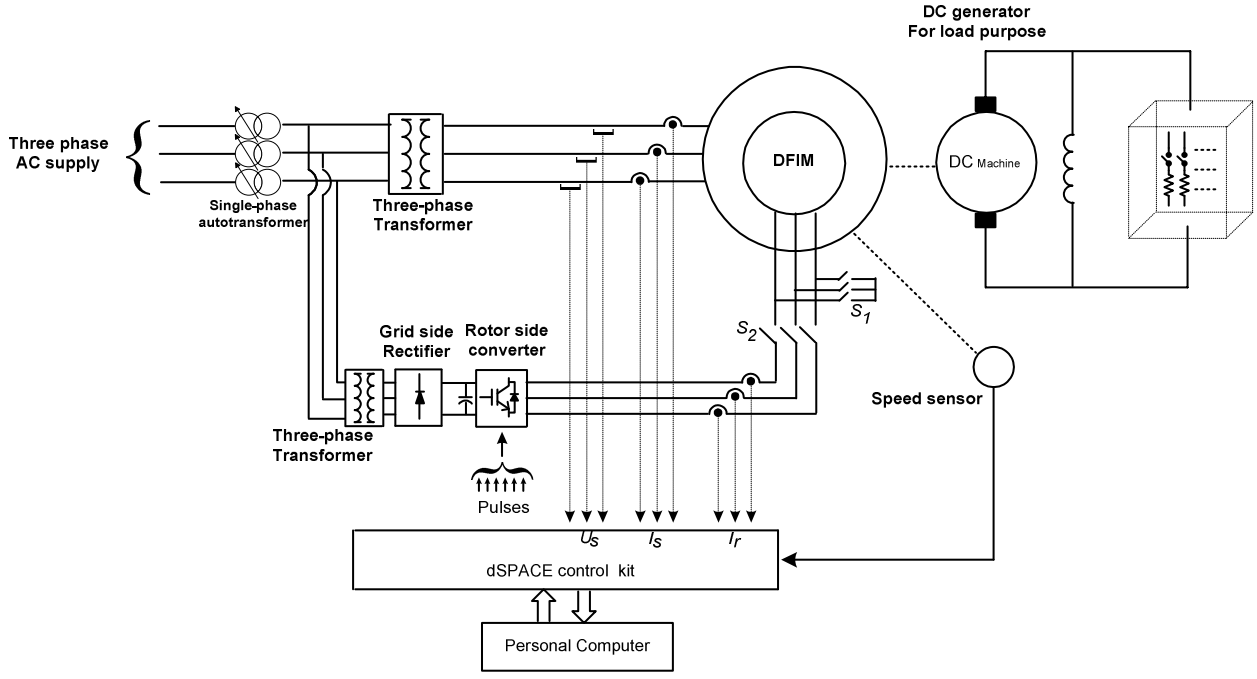

Fig. 2 Experimental set-up for DFIM tests

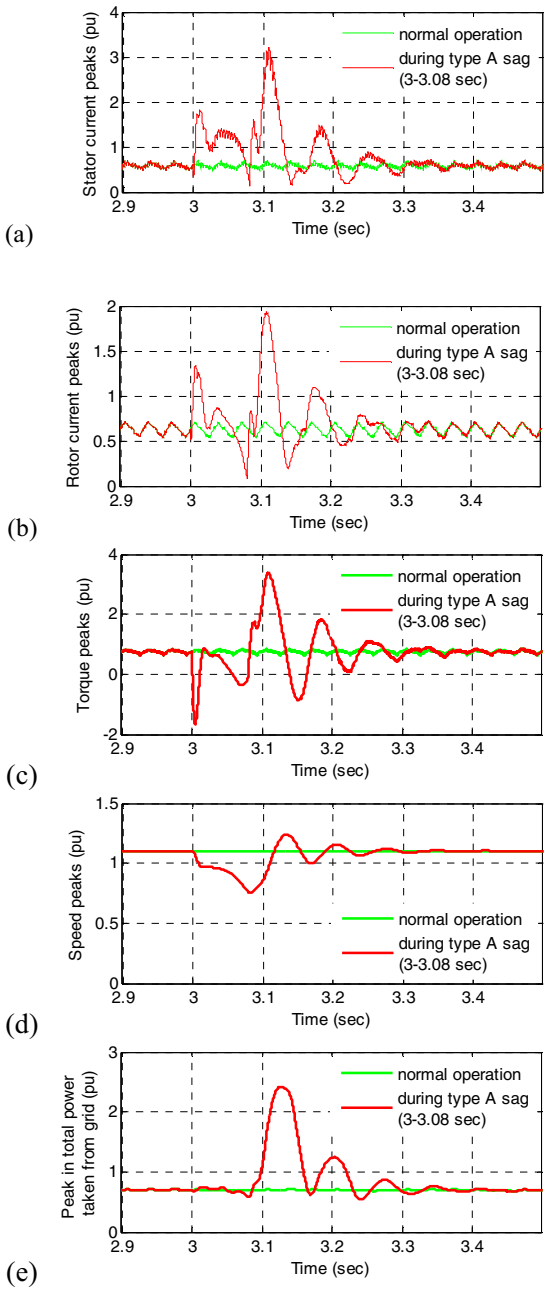

Fig. 3 comparison of on-sag and post sag peaks at load =0.75pu and speed=1.1pu for symmetrical type-A (abrupt) sag h=0.5, Δt=4T (3.00 – 3.08 sec), ψ=0° (a) stator phase currents (b) rotor phase currents (c) torque (d) speed (e) total power taken from grid

Fig. 4(a) shows speed profile and Fig. 4(b) shows rotor current profile during steady state condition, experimentally. The experimental RMS voltage magnitude and corresponding RMS stator current and total power taken from grid is illustrated in Fig. 5. Voltage sag depth (h=0.80), duration Δt=1sec is created in hardware, and corresponding peak in three-phase stator current, three-phase instantaneous power (total power taken from grid), rotor currents and grid side power factor are plotted in Fig. 5. 20% voltage dip creates around 80% increase in stator current, 38% increase in grid currents, 40% increase in total power and 40% reduction in overall power factor.

TABLE II. DFIM OPERATION WITH VARIOUS DEPTH AND DURATION

			Voltage sag depth								
			0.9	0.8	0.7	0.6	0.5	0.4	0.3	0.2	0.1
Symmetrical (type-A) voltage sag duration (cycles)	Instantaneous	0.5T	X	Y	Y	Y	Y	Y	Y	Y	Y
		1 T	X	Y	Y	Y	Y	Y	Y	Y	Y
		2 T	X	Y	Y	Y	Y	Y	Y	S	S
		3 T	X	Y	Y	Y	Y	Y	Y	S	S
		4 T	X	Y	Y	Y	Y	Y	S	S	S
		5 T	X	Y	Y	Y	Y	S	S	S	S
		10 T	X	Y	S	S	S	S	S	S	S
		15 T	X	Y	S	S	S	S	S	S	S
		20 T	X	Y	S	S	S	S	S	S	S
		25 T	X	Y	S	S	S	S	S	S	S
		30 T	X	Y	S	S	S	S	S	S	S

X=system is running without reduction in speed and torque
Y=system survives with significant reduction in speed and torque
S=system stall

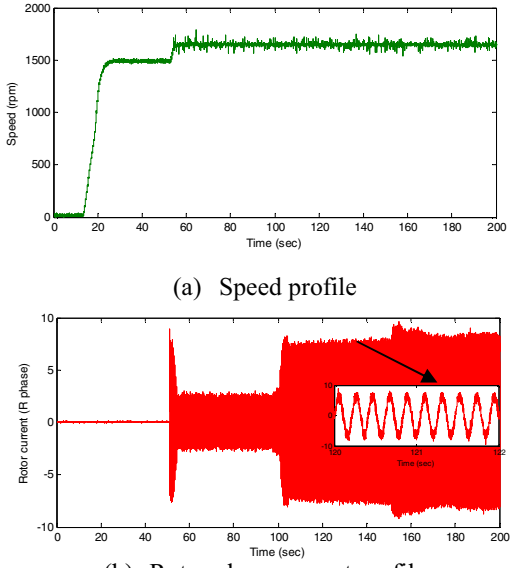

(a) Speed profile

(b) Rotor phase current profile

Fig. 4 Experimental results for starting and hyper-synchronous speed operation

V. CONCLUSION

The effects of symmetrical voltage sag on the performance of DFIM at hyper-synchronous motoring mode are investigated through simulation and hardware. Peaks in total power taken from grid, torque and current (stator and rotor current), and speed loss is plotted. DFIM stable region of operation is described for 0.75pu load and 1.1pu speed. Drive speed is affected badly during on-sag, whereas more peaks are obtained after sag in stator currents, rotor currents, torque and total power. High peak in rotor current may cause the failure of rotor side converter and power peaks may creates further dips for nearby equipment.

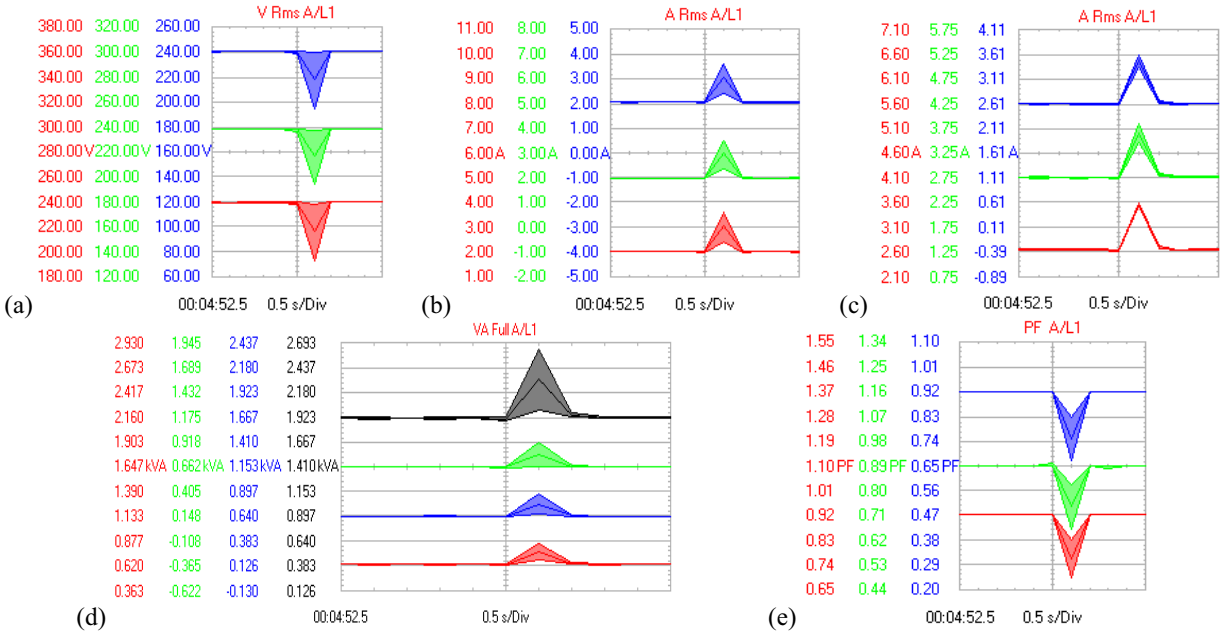

Fig. 5 Experimental results for h=0.80, Δt=1sec (a) RMS grid voltage (b) RMS three-phase stator currents (c) RMS three-phase grid currents (d) Total power taken from grid (e) overall grid side power factor

References

[1] Y. P. Verma and A. Kumar, "Potential impacts of emission concerned policies on power system operation with renewable energy sources," *International Journal of electrical power & energy systems,* vol. 44, pp. 520-529, 2013.

[2] G. Xydis, "Comparison study between a renewable energy supply system and a supergrid for achieving 100% from renewable energy sources in Islands," *International Journal of Electrical Power & Energy Systems,* vol. 46, pp. 198-210, 2013.

[3] C. Goodbody, E. Walsh, K. P. McDonnell, and P. Owende, "Regional integration of renewable energy systems in Ireland–the role of hybrid energy systems for small communities," *International Journal of Electrical Power & Energy Systems,* vol. 44, pp. 713-720, 2013.

[4] J. P. Barton and D. G. Infield, "Energy storage and its use with intermittent renewable energy," *Energy Conversion, IEEE Transactions on,* vol. 19, pp. 441-448, 2004.

[5] J. Kondoh, I. Ishii, H. Yamaguchi, A. Murata, K. Otani, K. Sakuta, *et al.*, "Electrical energy storage systems for energy networks," *Energy Conversion and Management,* vol. 41, pp. 1863-1874, 2000.

[6] J. Fraile-Ardanuy, J. R. Wilhelmi, J. J. Fraile-Mora, and J. I. Pérez, "Variable-speed hydro generation: operational aspects and control," *Energy Conversion, IEEE Transactions on,* vol. 21, pp. 569-574, 2006.

[7] E. Schmidt, J. Ertl, A. Preiss, R. Zensch, R. Schurhuber, and J. Hell, "Studies about the low voltage ride through capabilities of variable-speed motor-generators of pumped storage hydro power plants," in *Universities Power Engineering Conference (AUPEC), 2011 21st Australasian*, 2011, pp. 1-6.

[8] J.-J. Simond, A. Sapin, and D. Schafer, "Expected benefits of adjustable speed pumped storage in the European network," 1999.

[9] Y. Pannatier, B. Kawkabani, C. Nicolet, J.-J. Simond, A. Schwery, and P. Allenbach, "Investigation of control strategies for variable-speed pump-turbine units by using a simplified model of the converters," *Industrial Electronics, IEEE Transactions on,* vol. 57, pp. 3039-3049, 2010.

[10] E. Shehata and G. M. Salama, "Direct power control of DFIGs based wind energy generation systems under distorted grid voltage conditions," *International Journal of Electrical Power & Energy Systems,* vol. 53, pp. 956-966, 2013.

[11] I. P. Quality, "IEEE recommended practice for monitoring electric power quality," *IEEE recommended practice for monitoring electric power quality,* 1995.

[12] P. Gnacinski, "Energy saving work of frequency controlled induction cage machine," *Energy conversion and management,* vol. 48, pp. 919-926, 2007.

[13] M. H. Bollen, "Voltage recovery after unbalanced and balanced voltage dips in three-phase systems," *Power Delivery, IEEE Transactions on,* vol. 18, pp. 1376-1381, 2003.

[14] N. Kumar, T. R. Chelliah, and S. Srivastava, "Voltage sag effects on energy-optimal controlled induction motor with time-varying loads," in *Power Electronics, Drives and Energy Systems (PEDES), 2012 IEEE International Conference on*, 2012, pp. 1-6.

[15] W. Leonhard, *Control of electrical drives*: Springer, 2001.

[16] P. C. Krause, O. Wasynczuk, S. D. Sudhoff, and S. Pekarek, *Analysis of electric machinery and drive systems* vol. 75: John Wiley & Sons, 2013.

[17] A. Karthikeyan, C. Nagamani, A. R. Chaudhury, and G. Ilango, "Implicit position and speed estimation algorithm without the flux computation for the rotor side control of doubly fed induction motor drive," *Electric Power Applications, IET,* vol. 6, pp. 243-252, 2012.

[18] J. Yao, H. Li, Y. Liao, and Z. Chen, "An improved control strategy of limiting the DC-link voltage fluctuation for a doubly fed induction wind generator," *Power Electronics, IEEE Transactions on,* vol. 23, pp. 1205-1213, 2008.

[19] R. Pena, J. Clare, and G. Asher, "A doubly fed induction generator using back-to-back PWM converters supplying an isolated load from a variable speed wind turbine," in *Electric Power Applications, IEE Proceedings-*, 1996, pp. 380-387.

Appendix A

2.2 kW DFIM parameters

3 HP, 50 Hz, 4 pole machine
Stator: 415 V, 4.7 A, star-connected
Rotor: 185 V, 7.5 A, star-connected

Parameter	Symbol	Actual (SI unit)
Stator resistance	(R_s)	4.42 Ω
Rotor resistance	(R_r')	3.51 Ω Stator
inductance	(L_s)	323.21 mH
Rotor inductance	(L_r')	323.21 mH
Stator leakage inductance	(L_{ls})	25.71 mH
Rotor leakage inductance	(L_{lr}')	25.71 mH
Magnetizing inductance	(L_m)	297.5 mH
Machine rotor inertia	(J)	13.695 g m^2
Friction factor	(B)	0.033 g m^2/s
Number of poles pairs	(p)	2